



UNIVERSITY OF LEEDS

This is a repository copy of *Interactions of Asphaltene Subfractions in Organic Media of Varying Aromaticity*.

White Rose Research Online URL for this paper:

<http://eprints.whiterose.ac.uk/139427/>

Version: Accepted Version

---

**Article:**

Qiao, P, Harbottle, D orcid.org/0000-0002-0169-517X, Li, Z et al. (2 more authors) (2018) Interactions of Asphaltene Subfractions in Organic Media of Varying Aromaticity. *Energy & Fuels*, 32 (10). pp. 10478-10485. ISSN 0887-0624

<https://doi.org/10.1021/acs.energyfuels.8b02170>

---

© 2018 American Chemical Society. This is an author produced version of a paper published in *Energy & Fuels*. Uploaded in accordance with the publisher's self-archiving policy.

**Reuse**

Items deposited in White Rose Research Online are protected by copyright, with all rights reserved unless indicated otherwise. They may be downloaded and/or printed for private study, or other acts as permitted by national copyright laws. The publisher or other rights holders may allow further reproduction and re-use of the full text version. This is indicated by the licence information on the White Rose Research Online record for the item.

**Takedown**

If you consider content in White Rose Research Online to be in breach of UK law, please notify us by emailing [eprints@whiterose.ac.uk](mailto:eprints@whiterose.ac.uk) including the URL of the record and the reason for the withdrawal request.

# **Interactions of Asphaltene Subfractions in Organic Media of Varying Aromaticity**

Peiqi Qiao<sup>1</sup>, David Harbottle<sup>2</sup>, Zuoli Li<sup>1</sup>, Yuechao Tang<sup>1</sup> and Zhenghe Xu<sup>1</sup>

<sup>1</sup>Department of Chemical and Materials Engineering, University of Alberta, Canada

<sup>2</sup>School of Chemical and Process Engineering, University of Leeds, UK

## **ABSTRACT**

Whole asphaltenes were fractionated by extended-saturates, aromatics, resins and asphaltenes (E-SARA) analysis into four asphaltene subfractions: toluene-extracted interfacially active asphaltenes (T-IAA), toluene-extracted remaining asphaltenes (T-RA), heptol 50/50-extracted interfacially active asphaltenes (HT-IAA), and heptol 50/50-extracted remaining asphaltenes (HT-RA). The aggregation kinetics of fractionated asphaltenes measured by dynamic light scattering (DLS) showed that decreasing solvent aromaticity promoted asphaltene aggregation for all subfractions. In a given solvent, T-IAA exhibited the strongest aggregation tendency, followed by HT-IAA, then T-RA and HT-RA. Such differences were attributed to the higher oxygen and sulfur contents (highlighted in sulfoxide content) in IAA subfractions than RA subfractions, as confirmed by elemental analysis and X-ray photoelectron spectroscopy (XPS). The interaction forces between immobilized fractionated asphaltenes were measured using an atomic force microscope (AFM) to obtain a fundamental understanding of asphaltene interactions in organic media of varying aromaticity. The results showed that decreasing solvent aromaticity reduced steric repulsion and increased adhesion between asphaltenes with asphaltenes adopting a more compressed conformation. IAA subfractions, in particular T-IAA, exhibited higher adhesion forces than RA subfractions during separation of two asphaltene films in contact. The results of AFM colloidal force measurements were in good agreement with the DLS data. In spite of the small sulfoxide content in asphaltenes, the sulfoxide groups are believed to play a critical role in enhancing asphaltene aggregation in the bulk oil phase.

## 1. INTRODUCTION

Frequently quantified by SARA (Saturates, Aromatics, Resins and Asphaltenes) analysis, asphaltenes are defined as a solubility class of petroleum molecules being soluble in aromatic solvents such as toluene but insoluble in n-alkanes such as n-pentane or n-heptane.<sup>1</sup> Despite their applications in coating and paving, asphaltenes are generally considered a nuisance.<sup>2–4</sup> Their ability to self-associate and partition at oil-solid and oil-water interfaces is the root cause of several major issues encountered during oil production and processing. The adsorption of asphaltenes onto solid surfaces can i) change reservoir wettability and plug wellbores,<sup>5,6</sup> and ii) block pipelines and foul equipment,<sup>7</sup> thereby reducing oil recovery and potentially halting oil production. On the other hand, the adsorption of asphaltenes to the oil-water interfaces significantly contributes to the stabilization of undesirable water-in-oil (W/O) emulsions, which pose severe corrosion problems to pipelines and refining facilities due to salts and fine solids associated with emulsified water droplets.<sup>8–11</sup> These asphaltene-induced problems are closely related to the inevitable self-aggregation behavior of asphaltenes as a result of the strong adsorption of asphaltene aggregates at oil–water interfaces or onto mineral and metallic surfaces.<sup>1,2,12,13</sup>

As a result of such important practical implications, the aggregation of asphaltenes has been the subject of extensive investigations for several decades. Asphaltenes are able to self-assemble at very low concentrations and in a good solvent such as toluene.<sup>14</sup> Fluorescence spectroscopic studies showed the gradual aggregation of asphaltenes with increasing asphaltene concentration.<sup>15,16</sup> Molecular dynamic simulations confirmed the formation of complex asphaltene aggregates both in the bulk oil phase and at the oil–water interface.<sup>17–19</sup> Chacón-Patiño et al.<sup>20</sup> and Yang et al.<sup>21</sup> reported that the asphaltene subfractions enriched in archipelago structures exhibited a higher tendency of self-association than those enriched in island structures. Mullins et al. proposed a step-wise asphaltene aggregation model in which asphaltene molecules begin to form nanoaggregates of ~2 nm, followed by further association of nanoaggregates to form clusters of ~5 nm.<sup>22</sup> Gray et al. proposed that asphaltenes self-associate to form a three-dimensional “supramolecular assembly” as a result of multiple intermolecular interactions, including aromatic  $\pi$ – $\pi$  stacking, hydrogen bonding, acid–base interaction, metal coordination and association of hydrophobic pockets.<sup>23</sup>

Addition of an aliphatic solvent can greatly enhance asphaltene aggregation.<sup>24</sup> Sirota et al. reported that asphaltene molecules in a good solvent underwent a thermodynamic phase separation following the addition of an aliphatic solvent.<sup>25</sup> Wang et al. pioneered the colloidal force measurements between whole asphaltenes coated on silica in organic solvents of different aromaticity (toluene to n-heptane ratio) using an atomic force microscopy (AFM).<sup>26,27</sup> The increase of n-heptane was found to reduce long-range steric repulsion and induce weak adhesion between asphaltene molecules. Using mica as the substrate material, Natarajan et al. and Zhang et al. observed a similar trend when studying the molecular interactions between whole asphaltenes using a surface forces apparatus (SFA).<sup>28,29</sup> The addition of n-heptane reduced the steric repulsion between asphaltenes, accompanied by an increase in adhesion force. Asphaltene films adsorbed on mica were found to swell significantly in toluene in contrast to those films immersed in n-heptane.

As discussed more recently,<sup>30–32</sup> studying whole asphaltenes may restrict our ability to determine the physicochemical characteristics of the most interfacially active asphaltenes, i.e., the most troublesome asphaltene subfractions which preferentially deposit and partition at oil-solid<sup>33–35</sup> or oil-water<sup>31,36–40</sup> interfaces. The extended-SARA (E-SARA) analysis fractionates whole asphaltenes according to their interfacial behaviors and adsorption characteristics, allowing us to target specific asphaltene subfractions of varying interfacial activities.<sup>32</sup> Subramanian et al. fractionated whole asphaltenes using the E-SARA analysis by adsorbing asphaltenes onto calcium carbonate.<sup>34</sup> The authors showed that the asphaltene subfraction irreversibly adsorbed onto calcium carbonate exhibited the highest concentration of carbonyl and carboxylic acid groups, which agreed with the work of Clingenpeel et al.<sup>41</sup>

In our previous studies of E-SARA fractionation based on asphaltene adsorption at oil-water interfaces, a total of four different asphaltene subfractions were obtained using toluene and heptol 50/50 (a mixture of n-heptane and toluene at a 1:1 volume ratio) as the extracting solvent, respectively.<sup>40</sup> We found that the oxygenated groups, in particular sulfoxides, played a critical role in enhancing asphaltene adsorption at oil-water interfaces. Among the four asphaltene subfractions, the subfraction containing the highest amount of

sulfoxides exhibited the highest interfacial activity, formed the most rigid interfacial films and contributed significantly to the stabilization of W/O emulsions.

Despite their critical importance in understanding molecular mechanisms of asphaltene-induced problems, no study has considered the molecular interactions between such interfacially active asphaltenes. The complex asphaltene interaction could be better understood by studying and comparing asphaltene subfractions of different interfacial activities and compositions, paving the way to correlate specific chemical functionalities with certain interaction characteristics. In the current work, the four different asphaltene subfractions were obtained according to the procedure outlined in our earlier study.<sup>40</sup> Dynamic light scattering (DLS) was used to measure the aggregation behaviors of these fractionated asphaltenes in organic solvents of varying aromaticity, while AFM colloidal force measurements were conducted to understand the mechanisms of their molecular interactions. Combined with the detailed characterizations of fractionated asphaltenes through elemental analysis and X-ray photoelectron spectroscopy (XPS), the results from this study provide molecular insights into the role of key functional groups in controlling asphaltene interactions.

## 2. MATERIALS AND METHODS

### 2.1 Materials

Whole asphaltenes were precipitated at a 40:1 (mL/g) n-pentane/bitumen ratio from vacuum distillation feed bitumen provided by Syncrude Canada, Ltd. (Canada). Optima<sup>TM</sup>-grade n-pentane, Optima<sup>TM</sup>-grade toluene, Optima<sup>TM</sup>-grade n-heptane (Fisher Scientific, Canada) were used as received. Heptol 50/50 and heptol 70/30 were prepared by mixing n-heptane and toluene at a 1:1 and 7:3 volume ratio, respectively. DI water with a resistivity of 18.2 MΩ·cm was used throughout the study.

Asphaltene subfractions were obtained using the E-SARA fractionation method by adsorbing asphaltenes at oil-water interfaces. In brief, the W/O emulsion was prepared using DI water and whole asphaltene-in-solvent solution, agitated at 30 000 rpm for 5 min and allowed to stand still overnight. The supernatant was removed and the sediment cake

(settled water droplets) of the emulsion was washed with fresh solvent until its supernatant appeared colorless. The cleaned sediment cake was then dried in a vacuum oven at 60 °C to obtain the interfacially active asphaltene subfraction, termed IAA. The asphaltenes which remained in the organic phase were considered as remaining asphaltenes (RA). Based on the different organic solvents used in the E-SARA fractionation, two IAA subfractions and two corresponding RA subfractions were collected as follows: toluene-extracted interfacially active asphaltenes (T-IAA), toluene-extracted remaining asphaltenes (T-RA), heptol 50/50-extracted interfacially active asphaltenes (HT-IAA), and heptol 50/50-extracted remaining asphaltenes (HT-RA). Further details on the E-SARA fractionation of whole asphaltenes can be found in our previous study.<sup>40</sup>

## 2.2 Dynamic Light Scattering (DLS)

The aggregation behaviors of fractionated asphaltenes were studied using the DLS technique. The mean hydrodynamic radius ( $R_h$ ) of the particles (asphaltene aggregates) is correlated directly to their diffusion coefficient ( $D$ ) according to the Stokes–Einstein equation

$$D = \frac{kT}{6\pi R_h \eta} \quad (1)$$

where  $k$  is the Boltzmann constant,  $T$  is the temperature, and  $\eta$  is the viscosity of solvent. For Brownian particles, their diffusion coefficient ( $D$ ) is also related to their characteristic diffusion time ( $\tau_D$ ) through

$$D = \frac{1}{2\tau_D q^2} \quad (2)$$

where  $q$  is the scattering vector given by

$$q = (4\pi n/\lambda) \sin(\theta/2) \quad (3)$$

with  $n$  being the refractive index of the medium in which the asphaltenes are dispersed, and  $\lambda$  being the wavelength of the laser beam. The DLS technique can measure the time-dependent autocorrelation function  $G(\tau)$  of the scattered light, which is a function of the characteristic diffusion time  $\tau_D$  and the decay time  $\tau$  between the measurements as given by

$$G(\tau) = b[1 + \epsilon \exp\left(-\frac{\tau}{\tau_D}\right)] \quad (4)$$

where  $b$  is the baseline correlation level relative to the total light scattering intensity, and  $\epsilon$  is the coefficient which depends on the stray light and the aperture size. In the current study, aggregates of fractionated asphaltenes were found to exhibit Brownian motion with different diffusion rates. Combining Eqs. (1-4), the mean hydrodynamic radius  $R_h$  of the asphaltene aggregates can be deduced from the DLS data. In spite of the tendency for asphaltenes to interact with each other to form growing aggregates, the DLS is applicable to monitor the size of asphaltenes when the measurement time is much shorter than the characteristic aggregation time. Details of the DLS technique can be found in the relevant literature.<sup>42,43</sup>

A multifunctional ALV 5022 laser light scattering goniometer (ALV, Germany) in combination with an ALV SP-86 digital correlator (ALV, Germany) was used in the DLS experiments. A He–Ne laser with an output power of 22 mW was used as the light source. The optical cell was placed in an index-matching cell filled with high-purity, dust-free toluene. 2 mL of 0.04 g/L fractionated asphaltene-in-solvent (heptol 50/50 or heptol 70/30) solution was added into the optical cell. The asphaltene concentration of 0.04 g/L was chosen in this study to ensure that the fractionated asphaltenes do not precipitate in the solvents during the measurement. The scattering angle was set at 75° to minimize the effect of backscattering from the samples. The data acquisition time was chosen to be 60 s to ensure no significant changes in the aggregate size during the measurement interval, while retaining a good signal/noise ratio. The total measurement time was limited to 2 h to avoid the artifacts of aggregate sedimentation. A lag time of 1 min was allowed between any two consecutive measurements. All of the measurements were carried out at room temperature ( $22 \pm 0.2$  °C) and ambient pressure.

### 2.3 Elemental Analysis

A FLASH 2000 CHNS/O analyzer (Thermo Scientific, U.S.A.) was used to analyze the contents of carbon, hydrogen, nitrogen, sulfur and oxygen of asphaltene subfractions. The standard operational method recommended by the instrument manufacturer was followed. Asphaltene samples of ~5 mg were used for the analysis.

## **2.4 X-ray Photoelectron Spectroscopy (XPS)**

A Kratos Axis 165 spectrometer (Kratos, U.K.) equipped with a monochromatic Al K $\alpha$  X-ray source (1486.6 eV) at 15 kV anode potential and 20 mA emission current was used to perform XPS analysis on the asphaltene subfractions. All the XPS spectra were calibrated by the binding energy of Au 4f7/2 at 84.0 eV with reference to the Fermi level. Narrow scan spectra over the C 1s, S 2p, N 1s and O 1s regions were acquired with a pass energy of 20.0 eV and a dwell time of 200 ms. Casa XPS software was used to conduct peak deconvolutions and calculate the atomic concentrations.

## **2.5 Colloidal Force Measurement using Atomic Force Microscopy (AFM)**

AFM was used to measure the interaction forces between asphaltene subfractions in different organic solvents. Asphaltene subfractions were coated onto silica wafers and probe particles by dip-coating method. The silica wafers (NanoFab, University of Alberta, Canada) were cleaned using freshly prepared piranha solutions [3:1 (v/v) H<sub>2</sub>SO<sub>4</sub>/H<sub>2</sub>O<sub>2</sub>], soaked for 1 h and rinsed with DI water prior to their use. The AFM colloidal probe was made by attaching a silica microsphere ( $D \approx 9 \mu\text{m}$ , Whitehouse Scientific, U.K.) onto the apex of an AFM tipless silicon nitride cantilever (NP-O10, Bruker Scientific, U.S.A.) using a two-component epoxy glue (EP2LV, Master Bound, U.S.A.). The colloidal probes were kept under vacuum overnight and then exposed to an ultraviolet light for 30 min to remove residual organic contaminants. The spring constants of AFM cantilevers used in this study were  $\sim 0.24 \text{ N/m}$  and did not change significantly during the force measurements (<10%). Prior to the force measurements, the treated probes and silica wafers were immersed in 0.1 g/L fractionated asphaltene-in-toluene solutions for 1 h, after which they were washed with pure toluene and then dried with gentle nitrogen gas blow. The fractionated asphaltene-coated silica wafers and colloidal probes were used for AFM colloidal force measurements. The clean and fractionated asphaltene-deposited silica wafers were imaged in air with a silicon tip at a scan rate of 1 Hz in ambient conditions of temperature and humidity using a Bruker ICON AFM (Bruker Scientific, U.S.A.) in tapping mode.

Interaction forces between fractionated asphaltenes immobilized on silica wafers and colloidal probes in organic solvents of varying aromaticity were measured using the same Bruker Icon AFM. The approach and retract velocity of the colloidal probe was fixed at 1

$\mu\text{m}/\text{s}$ . Details of the AFM force measurement technique can be found in the open literature.<sup>44–47</sup> All interaction forces were normalized by the radius of the colloidal probe coated with the fractionated asphaltenes. Force measurements were conducted in toluene, heptol 50/50 and heptol 70/30 using a house-made liquid cell at a constant temperature of  $22 \pm 1^\circ\text{C}$  and ambient pressure. After the solvent was injected into the cell, the system was allowed to equilibrate for 15 min before initiating force measurements. A number of different surface locations on at least two independent samples for each asphaltene-asphaltene pair were chosen to ensure that representative interaction forces were captured.

### 3. RESULTS AND DISCUSSION

#### 3.1 Aggregation of Fractionated Asphaltenes Monitored by DLS

The aggregation kinetics of fractionated asphaltenes were studied by DLS. The hydrodynamic radii of the aggregates of different asphaltene subfractions were measured as a function of time. At a concentration of 0.04 g/L in heptol 50/50, the T-IIA subfraction was found to be more prone to aggregation than any other subfractions, as shown in Figure 1a. The hydrodynamic radii of T-IIA aggregates quickly increased from around 500 nm, the largest initial size amongst the four fractionated asphaltenes, to almost 1600 nm after 2 h. The increase in size of HT-IIA aggregates was slower than that of T-IIA, while no significant size increase was observed for T-RA and HT-RA aggregates during the measurement time. The RA subfractions showed a much lower tendency to aggregate than the IIA subfractions. As an effective precipitant for asphaltenes, increasing the n-heptane content from heptol 50/50 to heptol 70/30 led to increased aggregation rates and enlarged ultimate aggregate sizes, as shown in Figure 1b. However, in comparison with the two IIA subfractions, the extent of enhanced aggregation was much smaller for T-RA and HT-RA.

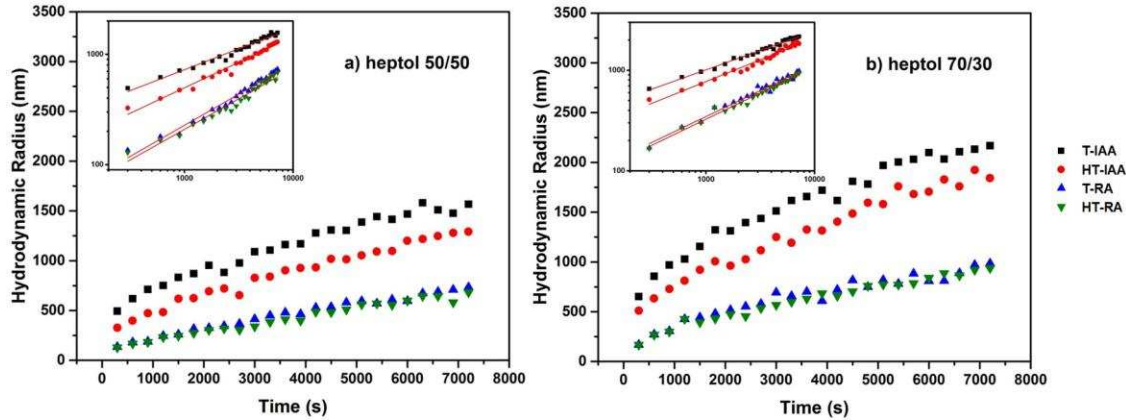


**Figure 1.** Time-dependent aggregation kinetics of 0.04 g/L fractionated asphaltenes in a) heptol 50/50 and b) heptol 70/30. Inset figures: data plotted on a log-log scale.

A linear relationship was observed between the hydrodynamic radii and aggregation time when plotted on a log-log scale (inset of Figure 1), indicating diffusion-limited aggregation for all asphaltene subfractions. The dependence of asphaltene aggregate size ( $R$ ) on time ( $t$ ) can be approximated as follows,

$$R = At^\alpha \quad (5)$$

where  $A$  is a constant determined by the size of initial asphaltene aggregates and the characteristic time of asphaltene nucleation.<sup>48</sup> The empirical fits showed that the T-RA and HT-RA had a similar  $\alpha$  of  $0.53 \pm 0.02$ , while  $\alpha$  was  $0.45 \pm 0.01$  and  $0.38 \pm 0.01$  for HT-IAA and T-IAA, respectively. The  $\alpha$  of T-IAA was similar to the value reported for whole asphaltenes ( $0.36 \pm 0.04$ ),<sup>48</sup> suggesting that the T-IAA subfraction contributes significantly to asphaltene aggregation despite the fact that T-IAA accounts for only a small fraction of the whole asphaltenes as shown by its low fractional yield ( $1.1 \pm 0.3$  wt%), see Table 1.

The differences in oxygen and sulfur contents among asphaltene subfractions caused their contrasting aggregation behaviors. The IAA subfractions, particularly T-IAA subfraction, featured higher oxygen and sulfur contents than RA subfractions (Table 1). As determined by elemental analysis, the oxygen content of T-IAA was ~1.5 times greater than that of HT-IAA, and 3 times greater than those of both RA subfractions. Such significant differences in oxygen and sulfur content were highlighted by the higher content of oxygenated polar groups, in particular sulfoxides, present in IAA subfractions than RA

subfractions, as verified by XPS analysis given in Table 1. The higher amount of sulfoxides in IAA provide more binding sites among IAA molecules than RA molecules, leading to a higher probability of aggregation and hence larger aggregates of IAA than RA through polar/hydrogen binding. It is therefore reasonable to conclude that the polar sulfoxides significantly contribute to promoting asphaltene aggregation, as supported by previous studies showing that considerably larger asphaltene aggregates were formed by the more polar asphaltene subfractions.<sup>49</sup> Using isothermal titration calorimetry (ITC), Subramanian and co-workers reported that the asphaltene subfraction with higher concentrations of polar groups (carbonyl, carboxylic acid or derivative groups) had a significantly higher aggregation tendency than other subfractions.<sup>35</sup> Similar results were also observed by Wang et al. using DLS.<sup>50</sup> The subfraction which was believed to be responsible for the aggregation of whole asphaltenes had the largest number of polar groups. The role of polar groups in enhancing asphaltene aggregation was also confirmed in studies of asphaltene model compounds.<sup>50</sup> In addition, by disrupting the interactions between the polar groups of asphaltene molecules, polar resins were found to be able to disperse asphaltenes.<sup>51</sup>

**Table 1.** Elemental composition of the four asphaltene subfractions.

	T-IAA	HT-IAA	T-RA	HT-RA
H/C ratio	1.19	1.20	1.18	1.18
N (wt%)	1.12	1.13	1.12	1.12
O (wt%)	5.64	3.70	1.38	1.33
S (wt%)	9.76	9.71	8.75	8.72
Sulfoxide (%) <sup>a</sup>	22.36	19.22	n/a	n/a
Fractional yield (wt%)	1.1 ± 0.3	4.2 ± 0.3	98.9 ± 0.3	95.8 ± 0.3

<sup>a</sup>Sulfoxide content determined by the peak area ratio of sulfoxide from the XPS S 2p band of each fractionated asphaltenes.

### 3.2 Characterization of Fractionated Asphaltene Films Deposited on Silica Wafers

Fractionated asphaltenes were coated onto silica wafers and colloidal probes in order to measure the interaction forces between asphaltene surfaces in organic media using an AFM. The successful and similar coatings of fractionated asphaltenes on both silica wafers and probes were confirmed by the identical interaction forces measured by AFM upon

approach between asphaltene-coated wafer-bare probe, and bare wafer-asphaltene-coated probe pairs.<sup>26,27</sup> The morphological features of the asphaltene films dip-coated from asphaltene solutions onto silica wafers were characterized in air by AFM in tapping mode (Figure 2). In reference, the bare hydrophilic silica wafer was flat and featureless, as shown in Figure 2a. In comparison, deposited asphaltenes following rinsing with pure toluene exhibited a layer of asphaltene aggregates of irregular shapes, suggesting a strong irreversible adsorption of asphaltenes onto hydrophilic silica surfaces (Figure 2b-2e). Asphaltene aggregates of equivalent diameter between 60 and 180 nm were observed for the HT-RA and T-RA, while the size of aggregates formed by HT-IIAA and T-IIAA increased to between 200 and 400 nm, with the aggregates much more densely distributed. The root mean square roughness ( $R_q$ ) of the dry asphaltene film gradually increased from ~1.1 to ~1.8 nm in the order of HT-RA, T-RA, HT-IIAA and T-IIAA. The results indicated the stronger aggregation of two IIAA subfractions than RA subfractions, which agrees well with the DLS data.

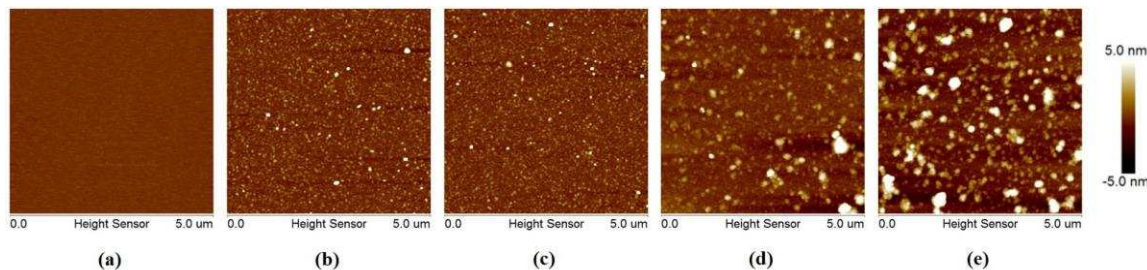


**Figure 2.** Tapping mode AFM imaging in air of clean bare silica surface (a) and silica surfaces coated with (b) HT-RA, (c) T-RA, (d) HT-IIAA and (e) T-IIAA.

Asphaltenes adsorb onto silica surfaces primarily through their polar functional groups.<sup>52,53</sup> The sulfoxide group was considered the single identifier for IIAA subfractions<sup>40</sup> with the T-IIAA containing more sulfoxides than the HT-IIAA (Table 1). The presence of polar oxygenated functional groups allows the asphaltene molecules to arrange themselves more favorably on hydrophilic solid surfaces<sup>53,54</sup> and oil-water interfaces,<sup>12,39,40</sup> mainly through hydrogen bonding interactions. It is therefore not surprising to see that T-IIAA molecules packed more densely on the hydrophilic silica surface than any other subfractions, resulting in the closest packing pattern amongst the four asphaltene subfractions.

### 3.3 Interaction Forces between Fractionated Asphaltenes in Organic Solvents

The interaction forces between immobilized asphaltene subfractions in toluene, heptol 50/50 and heptol 70/30 were measured using the AFM colloidal probe technique, to provide a fundamental understanding of asphaltene interactions in organic media. During approach, pure repulsion between two immobilized asphaltene surfaces was measured for all asphaltene subfractions. Since the electrostatic double-layer forces can be considered negligible in organic media, the observed repulsion was attributed to the steric repulsion between the immobilized asphaltene films.<sup>26</sup> Such interaction can be analyzed using the Alexander-de Gennes (AdG) scaling model, as asphaltenes exhibit similar steric interactions as swollen polymer brushes.<sup>26-29</sup> The AdG model is normally used to interpret the steric forces between surfaces coated with monodisperse and neutral polymer brushes in good solvents.<sup>55,56</sup> Since the absolute distance between the two asphaltene films is unknown in the AFM force measurements, the AdG model was modified to include a parameter  $\xi$  which describes the thickness of a fully compressed asphaltene film as follows,<sup>26,27</sup>

$$\frac{F(D)}{R} = \frac{16\pi k T L}{35 s^3} \left[ 7 \left( \frac{2L}{D + 2\xi} \right)^{5/4} + 5 \left( \frac{D + 2\xi}{2L} \right)^{7/4} - 12 \right]$$

for  $D + 2\xi < 2L$  (6)

where  $D$  is the distance between the probe and flat silica surface,  $R$  is the radius of the probe,  $k$  is the Boltzmann constant,  $T$  is the temperature,  $L$  is the length of protruding asphaltenes without compression,  $s$  is the average distance between two grafting points on the surface, and  $\xi$  is the thickness of a fully compressed asphaltene film (Figure 3).

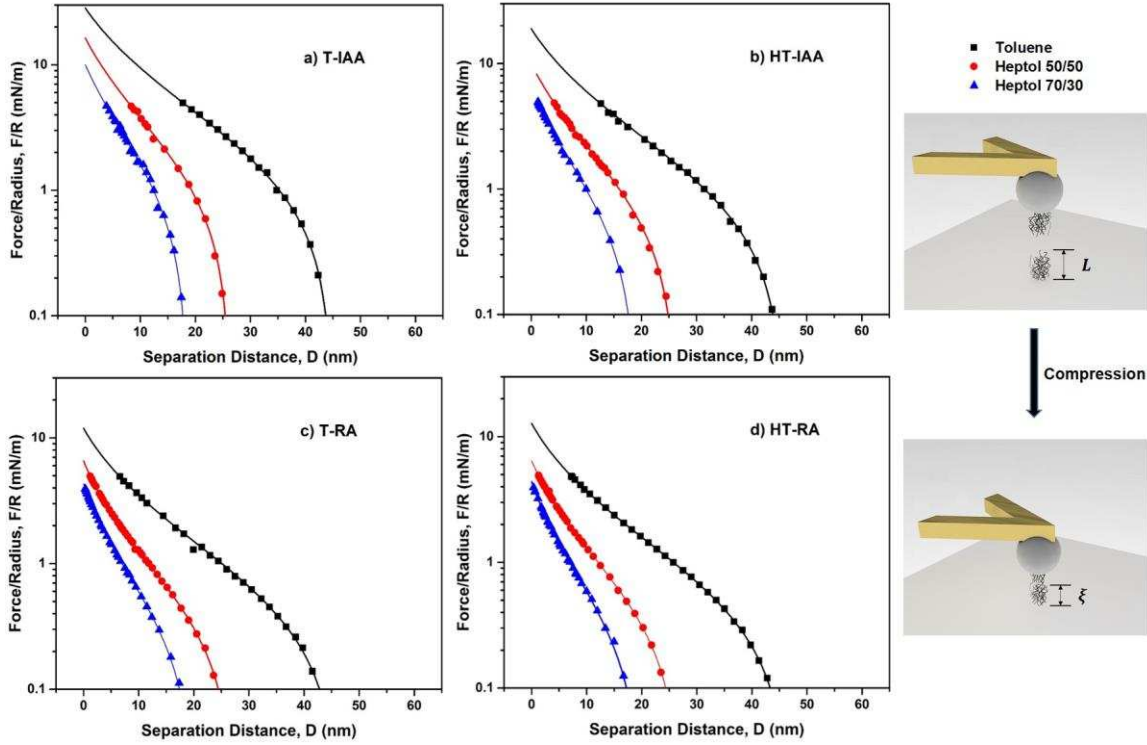


**Figure 3.** Measured force profiles (symbols) between two approaching fractionated asphaltene films (subfraction labelled in figure) immobilized on a silica colloidal probe and a flat silica substrate, respectively, in comparison with the best theoretical fit (solid lines) of the AdG model. Only one typical force profile has been reported for each condition to provide a clear illustration of the subfraction and solvent effect.

The measured repulsion was in good agreement with the AdG scaling model for all the cases (Figure 3), confirming that steric repulsion was the dominant interaction between asphaltene films during approach. Table 2 provides a summary of the fitting parameters  $L$ ,  $s$  and  $\xi$  obtained for the four asphaltene subfractions under different conditions. The varying trends of the three fitting parameters are readily observed in Figure 4. For all the subfractions, the uncompressed size ( $L$ ) of asphaltene films decreased with increasing n-heptane concentration, indicating a more dense conformation of asphaltenes induced by the addition of a poor solvent (n-heptane). For instance,  $L$  for T-IAA was reduced significantly from 41.9 to 19.5 nm as the solvent was changed from a good solvent (toluene) to a relatively poor solvent (heptol 70/30). Similar observations were previously noted when studying the molecular interactions between whole asphaltenes.<sup>27,29</sup> Likewise,  $\xi$

which describes the thickness of a fully compressed asphaltene film, was greater in toluene than in heptol 50/50 and heptol 70/30, for all the asphaltene subfractions. The smaller and denser asphaltene aggregates are less likely to repel each other when brought into contact, as verified by the decreasing magnitude and range of repulsive forces with increasing n-heptane content in the solvent. In terms of the average distance between the two grafting points on the surface, the largest values of  $s$  were observed in toluene for all the cases, with only a slight reduction (~ 2%) observed between the cases of heptol 50/50 and heptol 70/30.

**Table 2.** Parameter values obtained by fitting the repulsive interactions (Figure 3) using the AdG model.

	Toluene			Heptol 50/50			Heptol 70/30		
	$L$	$\xi$	$s$	$L$	$\xi$	$s$	$L$	$\xi$	$s$
	(nm)	(nm)	(nm)	(nm)	(nm)	(nm)	(nm)	(nm)	(nm)
T-IAA	41.9	4.8	9.3	26.1	3.8	8.5	19.5	3.4	8.3
HT-IAA	42.0	4.4	11.1	25.8	3.6	10.2	19.1	2.9	10.1
T-RA	41.6	3.9	13.6	25.5	2.9	12.9	19.3	2.5	12.7
HT-RA	41.8	3.8	13.5	25.6	3.1	12.6	19.0	2.4	12.7

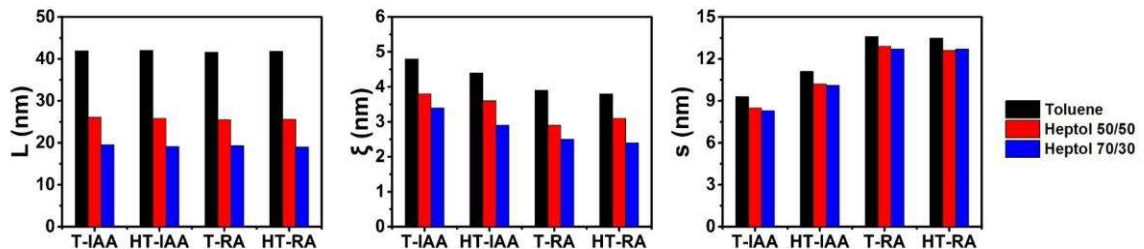


**Figure 4.** Varying trends of the AdG fitting parameters  $L$ ,  $\xi$  and  $s$  of the four asphaltene subfractions under different solvent conditions.

For different asphaltene subfractions under the same solvent conditions,  $L$  values were comparable, indicating little variation in the size of the uncompressed asphaltene films among the four subfractions. The fitted  $\xi$  values also showed little variation, all less than 5 nm which was close to the asphaltene film thickness ( $5 \pm 1$  nm) measured by ellipsometry

in air. The  $\xi$  values of the two IAA subfractions were slightly larger than those determined for the two RA subfractions in the same solvent. Such differences were anticipated due to the higher polarity of IAA subfractions and hence less compressible nature of their films.<sup>53</sup> Unlike  $L$  and  $\xi$ , the  $s$  values varied significantly among the different asphaltene subfractions. The RA subfractions showed larger  $s$  values than the IAA subfractions. For example, in heptol 50/50, the  $s$  values of T-RA and HT-RA were 12.9 and 12.6 nm, respectively, whereas the  $s$  values for HT-IAA and T-IAA were reduced to 10.2 and 8.5 nm, respectively. According to the definition,  $s$  represents the mean distance between the two neighboring grafting points on the surface. Since polar interactions are the main mechanism for asphaltene adsorption onto silica,<sup>52,53</sup> more polar functional groups would lead to more grafting points of asphaltenes on the surface. The asphaltene subfraction with the highest polarity (number of polar groups) would hence exhibit the smallest  $s$  value. As discussed earlier, the primary difference among the four fractionated asphaltenes was the higher amount of sulfoxide groups present in the IAA subfractions. In comparison with the RA subfractions, the IAA subfractions also contained more of other oxygenated polar functional groups, such as carbonyl and hydroxyl groups, more so for T-IAA than HT-IAA.<sup>40</sup> The T-IAA subfraction was therefore expected to result in the smallest  $s$  value, followed by HT-IAA, and then the two RA subfractions. This trend was in good agreement with the order of fitted  $s$  values, indicating the predominant role of polar interactions in the adsorption of asphaltenes onto hydrophilic silica. As a result, the T-IAA molecules had the least freedom of movement on the silica, leading to their closest packing pattern, which was in good agreement with the results of AFM imaging (Figure 2).

Figure 5 shows the magnitude of the adhesion forces measured when separating two contacting immobilized asphaltene surfaces in toluene, heptol 50/50 and heptol 70/30. For all subfractions, adhesion forces between the immobilized asphaltene surfaces increased with increasing n-heptane content in the solvent. The fully expanded (swollen) asphaltene aggregates in toluene featured no adhesion (unmeasurable) between opposing asphaltene films upon separation. For instance, the adhesion force ( $F_{ad}/R$ ) between the T-IAA films was unmeasurable in toluene, while it increased to ~0.29 mN/m in heptol 50/50, and further increased to ~0.41 mN/m in heptol 70/30. Increased adhesion between asphaltenes in more

aliphatic solvents (addition of n-heptane) correlated well with the stronger aggregation tendency of asphaltenes in more aliphatic solvents measured by DLS (Figure 1).

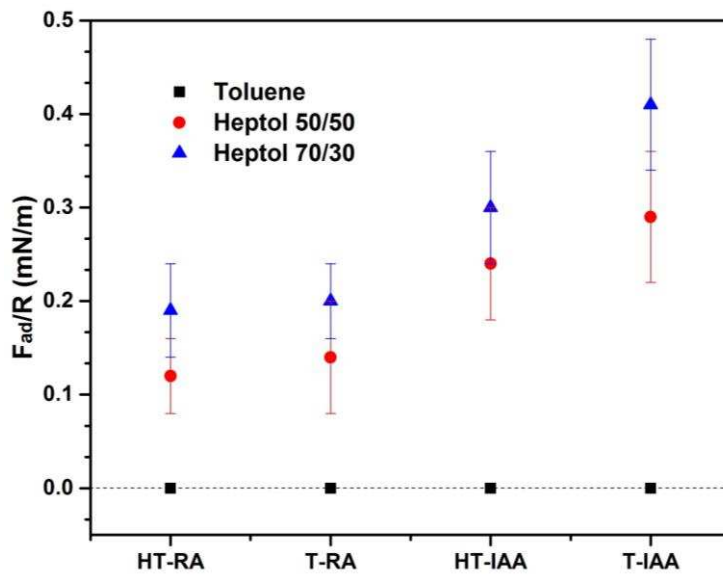


**Figure 5.** Normalized adhesion forces ( $F_{ad}/R$ ) between equivalent asphaltene subfractions interacting in toluene, heptol 50/50 and heptol 70/30. The dotted line indicates zero adhesion.

Under the same solvent conditions, T-IAA and HT-IAA exhibited larger adhesion forces than the two RA subfractions. The stronger adhesions between IAA subfractions were attributed to their higher oxygen and sulfur contents (Table 1). The heteroatoms (N, O and S) embedded in the aromatic rings of asphaltenes could strengthen the aromatic interaction between asphaltenes,<sup>17,57</sup> which is considered to be the dominant driving force for asphaltene aggregation.<sup>17,43,57,58</sup> The presence of heteroatoms increases the polarity of asphaltenes and hence enhances the  $\pi$ -electron cloud density of aromatic rings, thus contributing to stronger  $\pi-\pi$  stacking interactions between the polyaromatic cores of asphaltenes. In addition, heteroatoms along the aliphatic side chains of asphaltenes also play a significant role in the aggregation of asphaltenes through polar interactions.<sup>58-60</sup> The density functional theory (DFT) calculations by da Costa et al. showed that hydrogen bonding was as important as  $\pi-\pi$  interactions for asphaltene aggregation.<sup>61</sup> The higher oxygen and sulfur contents of the IAA subfractions can therefore be considered to be the primary cause for the enhanced association between neighboring asphaltenes. The AFM

colloidal force measurements correlated well with the aggregation trend revealed by DLS, confirming the stronger binding interactions between the IAA subfractions than the RA subfractions, as well as the role of n-heptane in enhancing asphaltene aggregation.

#### 4. CONCLUSION

The aggregation behaviors of four asphaltene subfractions (T-IAA, HT-IAA, T-RA and HT-RA) prepared using E-SARA fractionation were probed by DLS in organic media of varying aromaticity. The DLS results indicated a stronger aggregation tendency of the two IAA subfractions (especially T-IAA) than the two RA subfractions in a given solvent. Decreasing solvent aromaticity was found to promote asphaltene aggregation. AFM colloidal force measurements were conducted in order to obtain a molecular level understanding of asphaltene interactions, and the results showed a good correlation with the DLS findings. For all asphaltene subfractions, the solvent aromaticity significantly influenced the interaction forces between immobilized asphaltene films. As the solvent aromaticity decreased, asphaltene molecules adopted a more compressed conformation as verified by their collapsed sizes. The steric repulsion detected during the approach of two asphaltene films diminished with increasing n-heptane content. On the contrary, the adhesion forces measured during separation of two asphaltene surfaces in contact increased as the solvent changed from toluene to heptol 70/30. Under the same solvent conditions, IAA films were more likely to associate with each other than RA films as revealed during separation of two contacting asphaltene films. The greater aggregation tendency of IAA subfractions was attributed to their higher oxygen and sulfur contents. Compared with the RA subfractions, the presence of a larger number of oxygenated polar groups (particularly sulfoxides) greatly contributed to the stronger asphaltene aggregation by stronger  $\pi$ - $\pi$  interactions between large conjugated aromatic rings of asphaltenes, as well as hydrogen bonding interactions between polar groups of asphaltenes. The current study provides scientific insights into the molecular interactions between asphaltene molecules, specifically highlighting the contribution of sulfoxides which promote strong asphaltene aggregation.

## **ACKNOWLEDGEMENTS**

This research was conducted under the auspices of the Natural Sciences and Engineering Research Council (NSERC)–Industrial Research Chair (IRC) Program in Oil Sands Engineering. The partial support from Alberta Innovates Energy and Environmental Solutions and from National Natural Science Foundation of China (Grant 21333005) is also greatly appreciated.

## **REFERENCES**

- (1) Mullins, O. C. *Annu. Rev. Anal. Chem.* **2011**, 4, 393–418.
- (2) Akbarzadeh, K.; Hammami, A.; Kharrat, A.; Zhang, D.; Allenson, S.; Creek, J.; Kabir, S.; Jamaluddin, A. J.; Marshall, A. G.; Rodgers, R. P.; Mullins, O. C.; Solbakken, T. *Oilfield. Rev.* **2007**, 19, 22–43.
- (3) Adams, J. J. *Energy Fuels* **2014**, 28, 2831–2856.
- (4) Langevin, D.; Argillier, J.-F. *Adv. Colloid Interface Sci.* **2015**, 233, 83–93.
- (5) Drummond, C.; Israelachvili, J. J. *Pet. Sci. Eng.* **2004**, 45, 61–81.
- (6) Eskin, D.; Mohammadzadeh, O.; Akbarzadeh, K.; Taylor, S. D.; Ratulowski, J. *Can. J. Chem. Eng.* **2016**, 94, 1202–1217.
- (7) Torres, C.; Treint, F.; Alonso, C.; Milne, A.; Lecomte, A. *SPE/ICoTA Coiled Tubing Conf. Exhib. Woodlands, TX, April 12–13, 2005; SPE 93272.*
- (8) Yarranton, H. W.; Hussein, H.; Masliyah, J. H. *J. Colloid Interface Sci.* **2000**, 228, 52–63.
- (9) Kilpatrick, P. K. *Energy Fuels* **2012**, 26, 4017–4026.
- (10) Tchoukov, P.; Yang, F.; Xu, Z.; Dabros, T.; Czarnecki, J.; Sjöblom, J. *Langmuir* **2014**, 30, 3024–3033.
- (11) Harbottle, D.; Chen, Q.; Moorthy, K.; Wang, L.; Xu, S.; Liu, Q.; Sjöblom, J.; Xu, Z. *Langmuir* **2014**, 30, 6730–6738.
- (12) Teklebrhan, R. B.; Ge, L.; Bhattacharjee, S.; Xu, Z.; Sjöblom, J. *J. Phys. Chem. B*

**2014**, 118, 1040–1051.

- (13) Xiong, Y.; Cao, T.; Chen, Q.; Li, Z.; Yang, Y.; Xu, S.; Yuan, S.; Sjöblom, J.; Xu, Z. *J. Phys. Chem. C* **2017**, 121, 5020–5028.
- (14) Yarranton, H. W.; Ortiz, D. P.; Barrera, D. M.; Baydak, E. N.; Barré, L.; Frot, D.; Eyssautier, J.; Zeng, H.; Xu, Z.; Dechaine, G.; Becerra, M.; Shaw, J. M.; McKenna, A. M.; Mapolelo, M. M.; Bohne, C.; Yang, Z.; Oake, J. *Energy Fuels* **2013**, 27, 5083–5106.
- (15) Ghosh, A. K.; Srivastava, S. K.; Bagchi, S. *Fuel* **2007**, 86, 2528–2534.
- (16) Ghosh, A. K.; Chaudhuri, P.; Panja, S. S. *Fuel* **2016**, 185, 164–170.
- (17) Sedghi, M.; Goual, L.; Welch, W.; Kubelka, J. J. *Phys. Chem. B* **2013**, 117, 5765–5776.
- (18) Mikami, Y.; Liang, Y.; Matsuoka, T.; Boek, E. S. *Energy Fuels* **2013**, 27, 1838–1845.
- (19) Gao, F.; Xu, Z.; Liu, G.; Yuan, S. *Energy Fuels* **2014**, 28, 7368–7376.
- (20) Chacón-Patiño, M. L.; Rowland, S. M.; Rodgers, R. P. *Energy Fuels* **2018**, 32, 314–328.
- (21) Yang, F.; Tchoukov, P.; Dettman, H.; Teklebrhan, R. B.; Liu, L.; Dabros, T.; Czarnecki, J.; Masliyah, J.; Xu, Z. *Energy Fuels* **2015**, 29, 4783–4794.
- (22) Mullins, O. C. *Energy Fuels* **2010**, 2179–2207.
- (23) Gray, M. R.; Tykwinski, R. R.; Stryker, M.; Tan, X. *Energy Fuels* **2011**, 25, 3125–3134.
- (24) Yarranton, H. W. *J. Dispers. Sci. Technol.* **2005**, 26, 5–8.
- (25) Sirota, E. B.; Lin, M. Y. *Energy Fuels* **2007**, 21, 2809–2815.
- (26) Wang, S.; Liu, J.; Zhang, L.; Xu, Z.; Masliyah, J. *Energy Fuels* **2009**, 23, 862–869.
- (27) Wang, S.; Liu, J.; Zhang, L.; Masliyah, J.; Xu, Z. *Langmuir* **2010**, 26, 183–190.

- (28) Natarajan, A.; Xie, J.; Wang, S.; Liu, Q.; Masliyah, J.; Zeng, H.; Xu, Z. *J. Phys. Chem. C* **2011**, *115*, 16043–16051.
- (29) Zhang, L.; Shi, C.; Lu, Q.; Liu, Q.; Zeng, H. *Langmuir* **2016**, *32*, 4886–4895.
- (30) Czarnecki, J.; Tchoukov, P.; Dabros, T. *Energy Fuels* **2012**, *26*, 5782–5786.
- (31) Czarnecki, J.; Tchoukov, P.; Dabros, T.; Xu, Z. *Can. J. Chem. Eng.* **2013**, *91*, 1365–1371.
- (32) Qiao, P.; Harbottle, D.; Tchoukov, P.; Masliyah, J. H.; Sjöblom, J.; Liu, Q.; Xu, Z. *Energy Fuels* **2017**, *31*, 3330–3337.
- (33) Dudášová, D.; Simon, S.; Hemmingsen, P. V.; Sjöblom, J. *Colloids Surf., A* **2008**, *317*, 1–9.
- (34) Subramanian, S.; Simon, S.; Gao, B.; Sjöblom, J. *Colloids Surf., A* **2016**, *495*, 136–148.
- (35) Subramanian, S.; Humberstad, G.; Simon, S.; Xu, Z.; Sjöblom, J. *Colloids Surf., A* **2017**, *514*, 79–90.
- (36) Xu, Y.; Dabros, T.; Hamza, H.; Shefantook, W. *Pet. Sci. Technol.* **1999**, *17*, 1051–1070.
- (37) Wu, X. *Energy Fuels* **2003**, *17*, 179–190.
- (38) Yang, F.; Tchoukov, P.; Pensini, E.; Dabros, T.; Czarnecki, J.; Masliyah, J.; Xu, Z. *Energy Fuels* **2014**, *28*, 6897–6904.
- (39) Yang, F.; Tchoukov, P.; Dettman, H.; Teklebrhan, R. B.; Liu, L.; Dabros, T.; Czarnecki, J.; Masliyah, J.; Xu, Z. *Energy Fuels* **2015**, *29*, 4783–4794.
- (40) Qiao, P.; Harbottle, D.; Tchoukov, P.; Wang, X.; Xu, Z. *Energy Fuels* **2017**, *31*, 9179–9187.
- (41) Clingenpeel, A. C.; Rowland, S. M.; Corilo, Y. E.; Zito, P.; Rodgers, R. P. *Energy Fuels* **2017**, *31*, 5933–5939.
- (42) Hassan, P. A.; Rana, S.; Verma, G. *Langmuir* **2015**, *31*, 3–12.

- (43) Wang, W.; Taylor, C.; Hu, H.; Humphries, K. L.; Jaini, A.; Kitimet, M.; Scott, T.; Stewart, Z.; Ulep, K. J.; Houck, S.; Luxon, A.; Zhang, B.; Miller, B.; Parish, C. A.; Pomerantz, A. E.; Mullins, O. C.; Zare, R. N. *Energy Fuels* **2017**, *31*, 9140–9151.
- (44) Liu, J.; Xu, Z.; Masliyah, J. *Langmuir* **2003**, *19*, 3911–3920.
- (45) Liu, J.; Xu, Z.; Masliyah, J. *AIChE J.* **2004**, *50*, 1917–1927.
- (46) Liu, J.; Xu, Z.; Masliyah, J. *Colloids Surf., A* **2005**, *260*, 217–228.
- (47) Long, J.; Zhang, L.; Xu, Z.; Masliyah, J. H. *Langmuir* **2006**, *22*, 8831–8839.
- (48) Anisimov, M. A.; Ganeeva, Y. M.; Gorodetskii, E. E.; Deshabo, V. A.; Kosov, V. I.; Kuryakov, V. N.; Yudin, D. I.; Yudin, I. K. *Energy Fuels* **2014**, *28*, 6200–6209.
- (49) Spiecker, P. M.; Gawrys, K. L.; Kilpatrick, P. K. *J. Colloid Interface Sci.* **2003**, *267*, 178–193.
- (50) Wang, X.; Zhang, R.; Liu, L.; Qiao, P.; Simon, S.; Sjöblom, J.; Xu, Z.; Jiang, B. *Energy Fuels* **2017**, *31*, 9201–9212.
- (51) Spiecker, P. M.; Gawrys, K. L.; Trail, C. B.; Kilpatrick, P. K. *Colloids Surf., A* **2003**, *220*, 9–27.
- (52) Hannisdal, A.; Ese, M.-H.; Hemmingsen, P. V.; Sjöblom, J. *Colloids Surf., A* **2006**, *276*, 45–58.
- (53) Abudu, A.; Goual, L. *Energy Fuels* **2009**, *23*, 1237–1248.
- (54) Pernyeszi, T.; Dékány, I. *Colloids Surf., A* **2001**, *194*, 25–39.
- (55) de Gennes, P. G. *Adv. Colloid Interface Sci.* **1987**, *27*, 189–209.
- (56) Butt, H. J.; Kappl, M.; Mueller, H.; Raiteri, R.; Meyer, W.; Ruhe, J. *Langmuir* **1999**, *15*, 2559–2565.
- (57) Wang, H.; Xu, H.; Jia, W.; Liu, J.; Ren, S. *Energy Fuels* **2017**, *31*, 2488–2495.
- (58) Goual, L.; Sedghi, M.; Wang, X.; Zhu, Z. *Langmuir* **2014**, *30*, 5394–5403.
- (59) Gawrys, K. L.; Blankenship, G. A.; Kilpatrick, P. K. *Energy Fuels* **2006**, *20*, 705–

714.

- (60) Sodero, A. C. R.; Santos Silva, H.; Guevara Level, P.; Bouyssiere, B.; Korb, J. P.; Carrier, H.; Alfarra, A.; Bégué, D.; Baraille, I. *Energy Fuels* **2016**, *30*, 4758–4766.
- (61) da Costa, L. M.; Stoyanov, S. R.; Gusarov, S.; Tan, X.; Gray, M. R.; Stryker, J. M.; Tykwiński, R.; De M. Carneiro, J. W.; Seidl, P. R.; Kovalenko, A. *Energy Fuels* **2012**, *26*, 2727–2735.